Photonic Signal Processing on Electronic Scales: Electro-Optical Field-Effect Nanoplasmonic Modulator

A. V. Krasavin* and A. V. Zayats

Department of Physics, King's College London, Strand, London WC2R 2LS, United Kingdom

(Received 9 November 2011; published 31 July 2012)

We develop a highly efficient approach for the modulation of photonic signals at the nanoscale, combining an ultrasubwavelength plasmonic guiding scheme with a robust electroabsorption effect in degenerate semiconductors. We numerically demonstrate an active electro-optical field-effect nanoplasmonic modulator with a revolutionary size of just $25 \times 30 \times 100$ nm^3, providing signal extinction ratios as high as 2 at switching voltages of only 1 V. The design is compatible with complementary metal-oxide-semiconductor (CMOS) technology and allows low-loss insertion in standard plasmonic and Si-photonic circuitry.

DOI: 10.1103/PhysRevLett.109.053901 PACS numbers: 42.82.Fv, 42.70.Nq, 42.79.Ta, 73.20.Mf

The introduction of broadband optical signals in telecommunications has led to unprecedentedly high signal transmission rates that were unachievable in the electronic domain [1,2]. At present, at the other end of the dimension scale, nanophotonics presents a new paradigm for high-speed data transfer by the implementation of hybrid electronic-photonic circuits, where on such electronic chips data transmission using light instead of electric signals to boost the data exchange rates [3,4].

A variety of Si-based photonic waveguides have recently been proposed to act as possible optical interconnects for both external and internal electronic chip communications [5–8]. The use of surface plasmon polaritons (SPPs), which are surface electromagnetic waves coupled to electron oscillations in metal [9], offers a unique opportunity to go even further and realize truly nanoscale photonic components, overcoming the diffraction limit of light and enabling the manipulation of photonic signals at the nanometer integration level approaching the modern electronics length scales [10,11]. A wide variety of plasmonic and metamaterial-based waveguides and components have since been proposed [12–21] in the development of this idea.

However, it will only be possible to envisage nanophotonics in the same way as electronics if nanoscale components for switching and modulating are implemented. Traditional approaches that rely on small refractive index changes of the material forming the active components require long propagation distances to accumulate the sufficient phase or absorption changes, which results in a device size of several micrometers, even in optimal device geometries [22–24]. Active control of light at the nanoscale calls for new approaches to enhance light-matter interaction, new nonlinear (meta)materials, and component designs [25–30]. Finally, such components need to be integrated in planar photonic circuitry, either Si or plasmonic based.

Here, we combine a truly nanoscale guiding approach based on plasmonic waveguides with a robust modulation principle, utilizing a highly efficient electro-optical material. Exploiting these advantages, we numerically demonstrate an active electro-optical field-effect plasmonic modulator with an unprecedentedly small size of $25 \times 30 \times 100$ nm^3. This is followed by a discussion of device integration into Si-photonic and plasmonic circuitry. This active nanophotonic component can be constructed on a technological platform fully compatible with complementary metal-oxide-semiconductor (CMOS) fabrication processes and, as such, is a qualitatively new step in the area of integrated photonics, combining the high integration density and functionality of electronic circuits with the superior bandwidth of photonic circuits.

In order to achieve a nanoscale device size and also ensure a strong interaction of the electromagnetic wave with the nanoscale active layer required for signal control, a wire-MIM (metal-insulator-metal) plasmonic guiding approach has been implemented. The waveguide consists of a 25×25 nm^2 aluminum wire separated from an aluminum chassis by a 5 nm HfO_2 spacer and is embedded in SiO_2 [Fig. 1(b)]. Such dimensions are at the forefront of modern electronic chip fabrication technology for local interconnects. The waveguide geometrical parameters were chosen taking into account the need for a strongly localized mode with an adequate propagation length and a high sensitivity to refractive index changes in the gap, in order to provide efficient modulation. Eigenmode numerical simulations show robust performance of such waveguiding structure [Fig. 1(b)]: at a telecommunication wavelength $\lambda = 1550$ nm, the plasmonic mode is predominantly localized in a region of just 25×5 nm^2 ($\sim 0.015\lambda \times 0.003\lambda$) and has a propagation length of $L_{\mathrm{prop}} \sim 420$ nm. High contrast between the real part of the mode effective refractive index [$\mathrm{Re}(n_{\mathrm{eff}}) = \mathrm{Re}(k_{\mathrm{mode}}/k) = 4.991$, $k = 2\pi/\lambda$ is the free space wave vector] and the refractive index of the dielectric environment ($n_{\mathrm{SiO_2}} = 1.444$) ensures the small size of the waveguide components (couplers to the low-loss dielectric or plasmonic waveguides, waveguide bends, etc.) with negligible signal leakage. Finally, the localization of the mode in the dielectric region between

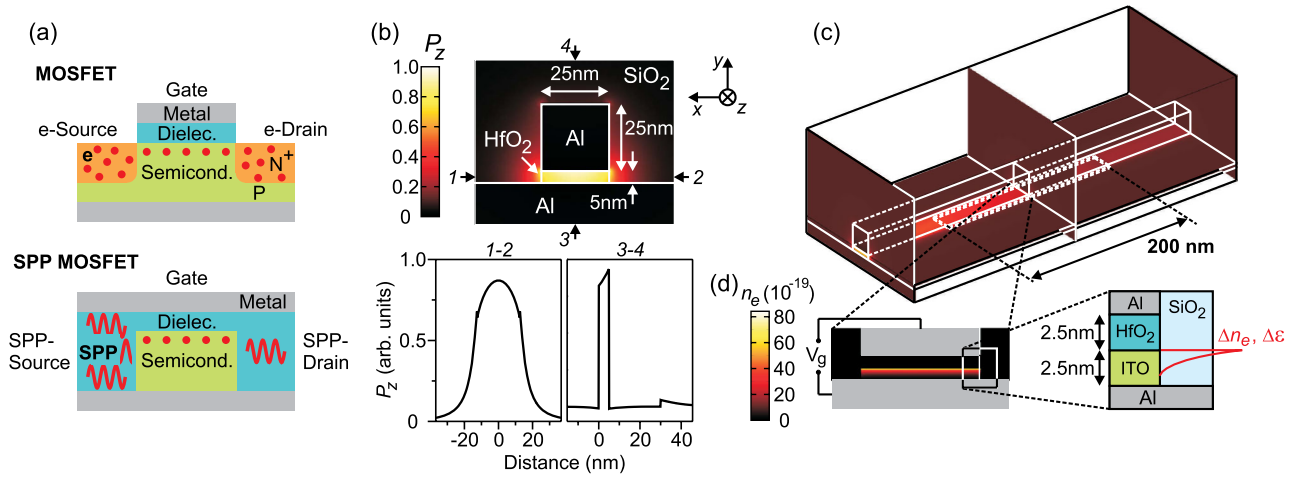

FIG. 1 (color online). Design and principle of operation of field-effect nanoplasmonic modulator. (a) Analogy between an electronic MOSFET transistor and the proposed plasmonic modulator. (b) Power flow profile of an SPP mode in a nanowire-MIM waveguide along with the vertical and horizontal cross sections. The nanowire size is 25×25 nm^2. (c) Map of the power flow P_z through the modulator at $V_g = 2$ V. (d) Electron density at $V_g = 2$ V obtained in self-consistent electrostatic simulations along with a zoom of the active region structure.

metals is particularly beneficial for utilizing electro-optic effects for signal modulation. Such structures can be fabricated on a fully CMOS compatible material platform and encapsulated on a chip.

The operating principle of the proposed nanoscale modulator is analogous to the operation of an electronic metal-oxide-semiconductor field-effect transistor (MOSFET), which forms the basis of contemporary CMOS technology. In MOSFET transistors, the flow of electrons from the input (source) to the output (drain) is controlled by the potential at the gate electrode, separated from the current channel by an insulating layer [Fig. 1(a), top sketch]. To realize the "on" state, the gate voltage attracts free carriers, forming an inversion conduction layer, therefore increasing current between source and the drain. In its plasmonic analogue, the input waveguide with optical power supplied in the form of highly localized SPP waves act as the SPP source, while the output SPP waveguide acts as the SPP drain. The voltage at the gate electrode controls the density of electrons at the semiconductor-dielectric interface in the very core of the waveguide. The SPP losses associated with these electrons are, thus, modulated, and therefore, the transmission of the SPP wave may be switched [Fig. 1(a), bottom sketch]. In this sense, the plasmonic modulator operates in a manner opposite to that of MOSFET, since higher electron density corresponds to higher SPP losses. By exploiting this pure plasmonic absorption approach rather than a photonic and plasmonic mode interference [31], a manyfold decrease in device size can be achieved, leading to efficient electronic-photonic integration.

To actively control plasmonic modes, the modulation of the refractive index in degenerate semiconductors [indium tin oxide (ITO)] has been used, an effect originating from changes in the free carrier concentration [31–33]. Even though this is the highest electro-optical effect observed so far, it has not been used in truly nanoscale systems. To estimate the effect, a 25 nm wide and 2.5 nm thick ITO stripe (free electron concentration $n_0 = 10^{19}$ cm^{-3}) was inserted at the bottom metal interface in the waveguiding area [Figs. 1(c) and 1(d)]. Numerical simulations show that under the application of a gate voltage of just 2 V across the gap region, an accumulation layer with a charge concentration as high as $n_e \sim 10^{21}$ cm^{-3} is produced at the ITO-HfO_2 interface. This modifies the plasma frequency

$$\omega_p = \sqrt{\frac{n_e q^2}{\epsilon_0 m^*}}, \tag{1}$$

where $\epsilon_\infty = 3.9$ is the high-frequency ITO permittivity [34], $m^* = 0.35 m_e$ is the effective mass of the electron [35], and q and m_e are the electron charge and mass. The change in carrier concentration, therefore, drastically changes the ITO permittivity in this region,

$$\epsilon_{\mathrm{ITO}} = \epsilon_\infty - \frac{\omega_p^2}{\omega^2 + i\omega\Gamma}. \tag{2}$$

Here $\Gamma = 1.8 \times 10^{14}$ rad/s is the ITO electron relaxation frequency [34]. The detailed description of the theoretical approach is given in the Supplemental Material [36]. By design, the nanoscale distribution of refractive index change has a strong spatial overlap with the localized plasmonic mode, resulting in both efficient modulation characteristics of the SPP mode and an ultrasmall device size. Eigenmode simulations of the ITO active region show that at a telecom wavelength of $\lambda = 1550$ nm, under application of a 2 V gate voltage, the propagation length of the mode decreases from ~400 to ~180 nm due to

increased imaginary part of the permittivity [determined by electron scattering (Ohmic) losses proportional to the increased free carrier concentration (Eqs. (1) and (2)]. Thus, the transmission through the structure is efficiently suppressed.

The ITO refractive index change [Eq. (2)] and the SPP mode profile, along with its propagation losses, are wavelength dependent. The change in mode propagation characteristics and ultimately the modulation of the signal are defined by an interplay between these parameters and consequently varies with wavelength. To find the wavelength region in which the SPP absorption change will be the most dramatic, for each wavelength the voltage was scanned, and the change in the mode effective refractive index as a function of applied gate voltage was monitored. At visible wavelengths the mode is naturally lossy, and its power flow distribution at higher voltages stays very similar to the distribution at zero voltage [Fig. 2(b), bottom left power flow map]. This is reflected in a smooth relative change in the effective refractive index of the mode [Fig. 2(a)] and a very limited relative change in its absorption [Fig. 2(b)]. At the same time in the infrared spectral range, the mode subject to much less loss initially [Fig. 2(b), top left power flow map] transforms into a very lossy mode at higher voltages due to the conductive electron accumulation layer and the increase in electron scattering associated with it. This leads to a complete change of the refractive index behavior and particularly to a drastic and sharp change in SPP absorption. Overall, the absorption is increased by almost a factor of 3. This change is much higher than the change in the real part of the mode effective refractive index (only a few percent), which calls for an absorption-based modulation approach rather than one based on phase modulation, with the infrared spectral region being ideal for this modulators operation (Fig. 2).

Based on these conclusions, further full three-dimensional finite element simulations of the SPP modulator based on this effect were performed at $\lambda = 1550$ nm. The active ITO region was extruded for 200 nm along the waveguide, producing a compact and technologically simple electrically controlled switching element [Fig. 1(b)]. The simulations show that a modulation gate voltage, V_{mod}, of just 1 V between the top wire and the bottom plane with a bias voltage $V_b = 1.2$ V, induces a twofold change in SPP mode transmittance (Fig. 3, solid black line; the voltage change region is marked by black vertical dotted lines). Because of the pure absorption mechanism of the modulation and negligible reflection from the device entrance ($\sim 3.5\%$ in the most extreme case of $V_g = 2.6$ V), the extinction of the device can be expressed as $\exp(-L/L_{\mathrm{mod}})$, where L is the modulator length and $L_{\mathrm{mod}} = 244$ nm is the characteristic modulation length. Therefore, longer modulators will have higher extinction

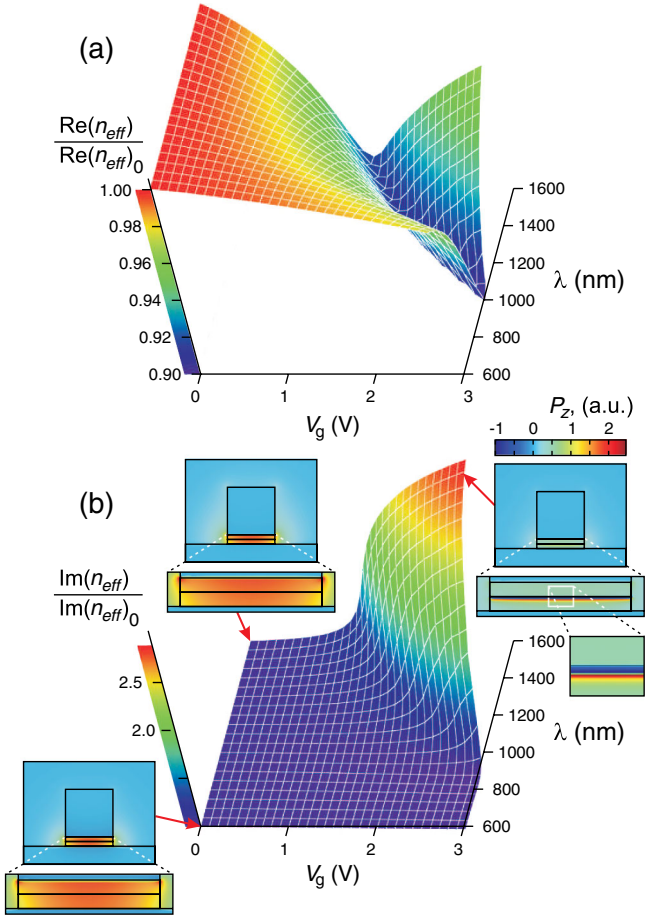

FIG. 2 (color online). Optimization of the wavelength range for modulator operation. (a) Real and (b) imaginary part of the effective refractive index of the SPP mode in the active region at various gate voltages V_g, normalized to the case of $V_g = 0$. Insets show power flow maps for selected wavelengths and gate voltages. The color scale is the same for all maps.

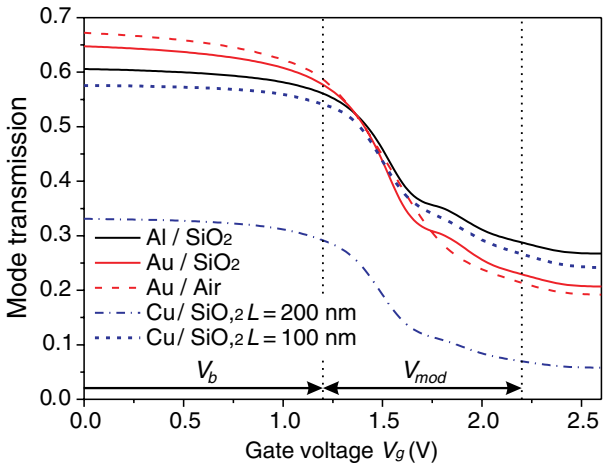

FIG. 3 (color online). Switching characteristic of the nanoplasmonic modulator. Transmission of the SPP mode through the modulator as a function of the gate voltage V_g for various material pairs. The transmission was calculated as a ratio of input and output power flows just after and just before the device.

ratios for the cost of generally lower output signal levels and larger device sizes. For example, for $L = 400$ nm an extinction ratio as high as 4 is predicted. Noticeable improvements in the performance of the device occurs if aluminum is replaced with gold [solid red (light gray in gray-scale) line], due to a stronger mode field localization in the gap. Also, the modulation remains high if the dielectric environment is changed to air [dashed red (light gray in gray-scale) line]. With the same underlying mechanisms, the effect is even more dramatic if Cu is used as the plasmonic material. The extinction ratio rises to a level of 4.2, or alternatively, the device can be made twice as short, while maintaining the same performance [Fig. 3, blue (dark gray in gray-scale) dash-dotted and short-dashed lines, respectively]. This results in a $25 \times 30 \times 100$ nm^3 active device providing manyfold signal modulation, the smallest photonic switching element proposed to date. In this work the optical constants of Cu, Au, and Al were taken from Palik [37]. It should be noted that the recent investigations of the Cu used in CMOS process [38,39] indicates that its optical properties may be comparable to those of Al in the telecom wavelength range. Finally, we note that the efficient interaction of the highly localized plasmonic mode with the nanoscale electron layer in this plasmonic switch driven by efficient absorption could also lead to nonlinear effects and all-plasmonic switching and, therefore, potentially to the realization of ultrafast all-plasmonic active circuitry [28,30].

An important parameter, determining the feasibility of device integration within a network of low-loss dielectric, Si-photonic, or plasmonic waveguides, is the insertion loss. Since nanoscale dimensions are at the very core of device operation, ensuring a good spatial overlap of the mode with the active layer and, therefore, a high-magnitude switching effect, coupling components for its integration in the above networks are needed. One of the possible approaches to integrate different sized waveguide components is the implementation of three-dimensional tapers that provide gradual modal evolution in both x and y directions. It has been implemented for transforming a 400×50 nm^2 mode in an ordinary MIM waveguide into the highly localized 25×5 nm^2 device mode (in-coupling scenario) and visa versa (out-coupling scenario). The in- and out-coupling efficiencies of the structures as a function of the tapering angle are presented in Fig. 4. The in-coupling efficiency (lower black curve) is determined by the tradeoff between total Ohmic losses increasing with longer propagation distances along the tapers with smaller opening angles and the radiation losses increasing for tapers with larger angles. The resulting maximum at $\alpha \sim 100°$ corresponds to an in-coupling efficiency as high as 65%. The out-coupling efficiency (upper red curve) monotonically increases up to values approaching 85% for large taper angles. Since the coupling between MIM and high-index Si-based waveguides and visa versa is in the region of 80–90% [40–42],

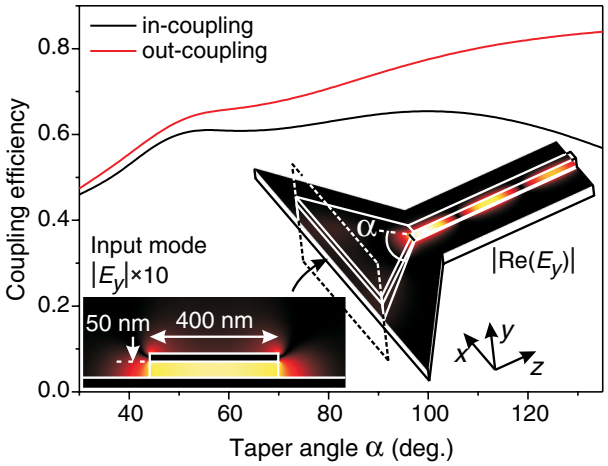

FIG. 4 (color online). Coupling efficiency between the 25×5 nm^2 core wire-MIM waveguide (Al/HfO_2 waveguide embedded in SiO_2) and a conventional 400×50 nm^2 core MIM waveguide with HfO_2 core (left inset) for tapers of various angles: (lower black curve) in-coupling and (upper red curve) out-coupling configurations. Inset: map of the field $|\mathrm{Re}(E_y)|$ coupled using a 90° taper and map of the input mode amplitude (scale increased by 10 times). The dashed rectangle shows the position of the silicon waveguide in the end-fire configuration.

the tapers can also be used for the incorporation of nanoplasmonic modulators into the silicon integrated waveguide circuitry. Even without any optimization or additional coupling structures, the end-fire in-coupling from the 400×300 nm^2 silica-coated Si waveguide (profile is outlined by the dashed rectangle in Fig. 4 inset) to the nanoplasmonic modulator using the taper was found to be 44%, for the reverse process (out-coupling) 22% (compared to the efficiencies of ~0.001% and ~0.1%, correspondingly, without the taper). In these simulations, to estimate coupling to the nanoscale mode, the structure, apart from the taper core, was shielded with a 50 nm metallic spacer. Summarizing, the total length of the nanoplasmonic modulator, including coupling tapers, can be below 500 nm, which is several times less then the best examples of plasmonic modulators [31], having a crucial advantage of integrable design.

In conclusion, we have demonstrated a truly nanoscale active nanoplasmonic modulator and developed a methodology of integration into plasmonic or dielectric photonic networks. From a scientific point of view, this is a fascinating and qualitatively new step towards manipulating and actively controlling light at the nanoscale. From a practical viewpoint, it is a potential breakthrough in the realization of broadband and potentially ultrafast active integrated circuits for the next generation of computational devices.

This work has been supported by EPSRC (U. K.). The authors acknowledge the fruitful discussions with Dr. Wayne Dickson and Dr. Daniel O'Connor.

*alexey.krasavin@kcl.ac.uk

[1] I. P. Kaminow, T. Li, and A. E. Willner, *Optical Fiber Telecommunications* (Academic, New York, 2008).
[2] D. Hillerkuss *et al.*, Nature Photon. **5**, 364 (2011).
[3] D. A. B. Miller, Proc. IEEE **88**, 728 (2000).
[4] A. Alduino *et al.*, in *Proceedings of the Integrated Photonics Research, Silicon and Nanophotonics, Monterey, California, 2010* (Optical Society of America, Washington, DC, 2010), p. PDIWI5.
[5] M. Lipson, J. Lightwave Technol. **23**, 4222 (2005).
[6] D. T. H. Tan, P. C. Sun, and Y. Fainman, Nature Commun. **1**, 116 (2010).
[7] G. Roelkens, L. Liu, D. Liang, R. Jones, A. Fang, B. Koch, and J. Bowers, Laser Photonics Rev. **4**, 751 (2010).
[8] K. Ohashi *et al.*, Proc. IEEE **97**, 1186 (2009).
[9] A. V. Zayats, I. I. Smolyaninov, and A. A. Maradudin, Phys. Rep. **408**, 131 (2005).
[10] *Plasmonic Nanoguides and Circuits*, edited by S. I. Bozhevolnyi (Pan Stanford, Singapore, 2008).
[11] S. A. Maier, *Plasmonics: Fundamentals and Applications* (Springer, New York, 2007).
[12] L. Liu, Z. Han, and S. He, Opt. Express **13**, 6645 (2005).
[13] S. A. Maier, M. L. Brongersma, P. G. Kik, S. Meltzer, A. A. G. Requicha, and H. A. Atwater, Adv. Mater. **13**, 1501 (2001).
[14] G. A. Wurtz, W. Dickson, D. O'Connor, R. Atkinson, W. Hendren, P. Evans, R. Pollard, and A. V. Zayats, Opt. Express **16**, 7460 (2008).
[15] E. Verhagen, M. Spasenovic, A. Polman, and L. (Kobus) Kuipers, Phys. Rev. Lett. **102**, 203904 (2009).
[16] J. Jung, T. Søndergaard, and S. I. Bozhevolnyi, Phys. Rev. B **76**, 035434 (2007).
[17] A. V. Krasavin and A. V. Zayats, Opt. Lett. **36**, 3127 (2011).
[18] A. V. Krasavin and A. V. Zayats, Opt. Express **18**, 11791 (2010).
[19] H.-S. Chu, E.-P. Li, P. Bai, and R. Hegde, Appl. Phys. Lett. **96**, 221103 (2010).
[20] A. Alu and N. Engheta, Phys. Rev. Lett. **103**, 143902 (2009).
[21] N. Engheta, Science **317**, 1698 (2007).
[22] A. V. Krasavin, S. Randhawa, J.-S. Bouillard, J. Renger, R. Quidant, and A. V. Zayats, Opt. Express **19**, 25222 (2011).
[23] J. Gosciniak, S. I. Bozhevolnyi, T. B. Andersen, V. S. Volkov, J. Kjelstrup-Hansen, L. Markey, and A. Dereux, Opt. Express **18**, 1207 (2010).
[24] A. V. Krasavin and A. V. Zayats, Appl. Phys. Lett. **97**, 041107 (2010).
[25] A. V. Krasavin and N. I. Zheludev, Appl. Phys. Lett. **84**, 1416 (2004).
[26] D. Pacifici, H. J. Lezec, and H. A. Atwater, Nature Photon. **1**, 402 (2007).
[27] R. Pala, K. T. Shimizu, N. A. Melosh, and M. L. Brongersma, Nano Lett. **8**, 1506 (2008).
[28] K. F. MacDonald, Z. L. Samson, M. I. Stockman, and N. I. Zheludev, Nature Photon. **3**, 55 (2008).
[29] G. A. Wurtz and A. V. Zayats, Laser Photonics Rev. **2**, 125 (2008).
[30] G. A. Wurtz, R. Pollard, W. Hendren, G. P. Wiederrecht, D. J. Gosztola, V. A. Podolskiy, and A. V. Zayats, Nature Nanotech. **6**, 107 (2011).
[31] A. Dionne, J. Diest, L. A. Sweatlock, and H. A. Atwater, Nano Lett. **9**, 897 (2009).
[32] E. Feigenbaum, K. Diest, and H. A. Atwater, Nano Lett. **10**, 2111 (2010).
[33] A. Melikyan *et al.*, Opt. Express **19**, 8855 (2011).
[34] F. Michelotti, L. Dominici, E. Descrovi, N. Danz, and F. Menchini, Opt. Lett. **34**, 839 (2009).
[35] J. R. Bellingham, W. A. Phillips, and C. J. Adkins, J. Phys. Condens. Matter **2**, 6207 (1990).
[36] See Supplemental Material at http://link.aps.org/supplemental/10.1103/PhysRevLett.109.053901 for more information on the theoretical approaches employed and material parameters.
[37] *Handbook of Optical Constants of Solids*, edited by E. D. Palik (Academic, New York, 1984).
[38] H. S. Lee, C. Awada, S. Boutami, F. Charra, L. Douillard, and R. Espiau de Lamaestre, Opt. Express **20**, 8974 (2012).
[39] S. Zhu, T. Y. Liow, G. Q. Lo, and D. L. Kwong, Opt. Express **19**, 8888 (2011).
[40] J. Tian, S. Yu, W. Yan, and M. Qiua, Appl. Phys. Lett. **95**, 013504 (2009).
[41] P. Ginzburg, D. Arbel, and M. Orenstein, Opt. Lett. **31**, 3288 (2006).
[42] R. A. Wahsheh, Z. Lu, and M. A. G. Abushagur, Opt. Express **17**, 19033 (2009).